

## A PLANAR MODEL OF HEPATIC BLOOD FLOW POTENTIAL

Hansjörg Scherberger<sup>1,2</sup> and Ortwin Leder<sup>1</sup>

<sup>1</sup>Anatomisches Institut II der Universität Freiburg, Albertstr. 17, D-79104 Freiburg, Germany

<sup>2</sup>To whom correspondence should be sent. Now at: Dept. of Neurology, Vestibular Lab., Zürich University Hospitals, CH-8091 Zürich, Switzerland

### ABSTRACT

We present a two-dimensional model of hepatic blood flow potential that takes afferent and efferent venous vessels and the sinusoidal capillary network into account. Congruent equilateral triangles were chosen as units. Planar patterns of such triangles can be interpreted in terms of the classical hexagonal liver lobule, a complementary bile lobule, and of Rappaport's acinus. Model assumptions include a fixed terminal portal and hepatic venous pressure and a fixed distribution of flow conductivity inside the planar unit. Simulated pressure potentials differed substantially for the physiologic condition and for liver congestion. The model corresponds to the planar distribution of glucose-6-phosphatase activity and demonstrates an intimate relationship between hepatic microcirculation and metabolic heterogeneity. Furthermore, in simulations of liver congestion, predicted alterations of intralobular pressure reflected changes of liver morphology, thus suggesting a causal association between both processes.

**Key words:** functional heterogeneity, blood circulation, liver congestion, simulation.

### INTRODUCTION

It is generally accepted that hepatic blood flow plays an important role in the organization of liver morphology and function. Though measurements of microvascular blood pressure are difficult to perform, some data about terminal portal and hepatic vein pressures exist (Ayuse et al., 1994; Greenway and Lauth, 1989; Laine et al., 1979; Lauth et al., 1986; McCuskey and Reilly, 1993; Mitzner, 1974; Nakata et al., 1960). Also, there is some information available about the diameter of sinusoidal capillaries (Wisse et al., 1985). However, a quantitative model of liver blood flow that could be compared with histological, histochemical, and pathological observations, is still lacking.

Considering perfusion data of the whole liver (Eisenberg, 1972), capillary blood flow might be quite slow and could be described as a potential flow, like water flowing through sand (Leder et al., 1991; Prandtl, 1956). Several two-dimensional schemes of functional liver units are well established. All of them are similar or complementary to the hexagonal model of a central vein lobule.

In an attempt to link these concepts, we present a planar model of microvascular blood flow potential based on an equilateral triangle with the terminal portal and venous pressure and the distribution of microvascular flow conductivity as free parameters.

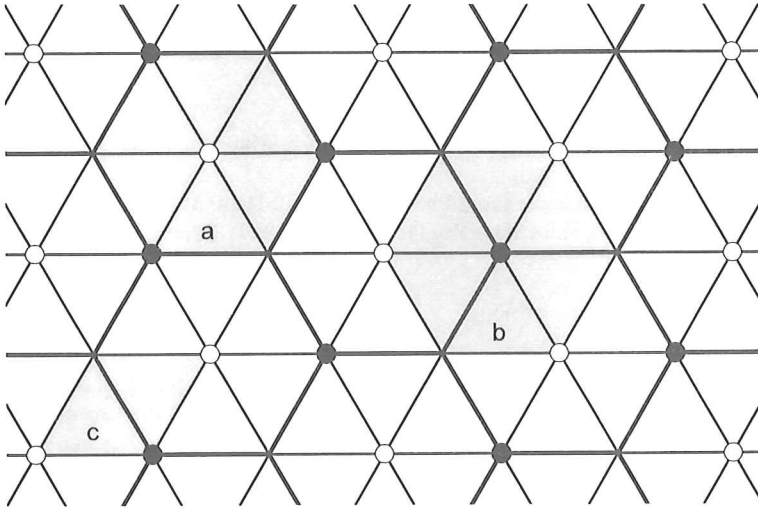


Fig. 1. Grid of unit-triangles in a section plane. Each equilateral unit-triangle contains a potential spring (dark spots) and a sink (white spots) in two corners whereas the third (free corner) has no predetermined potential. Hexagonal arrangement of unit-triangles around sinks (bold lines, a) correspond to the classical hexagonal liver lobule with a sink in the center and three springs alternating in the six corners of each hexagon. Complementary, hexagonal grouping around springs (b) conforms to the classical bile lobule model. Adjacent couples of unit triangles with a common spring and free corner (c) reflect the functional concept of

## Model

Centrolobular veins can easily be marked as sinks in the blood flow potential. Corresponding springs, in contrast, are more difficult to determine. In our approach we consider portal tracts as springs. Further, we model the course of terminal portal vessels by locally adapting the flow conductivity along the course of these vessels.

Geometric patterns of lobular cross sections are of irregular shape (Scherberger, 1996; Scherberger and Leder, 1997). For simplicity we based our model on an equilateral triangle. Each of these - in the following called unit-triangles - has a spring and a sink in two of its corners while the potential at the third corner, called *free corner*, is not predetermined. We consider the section plane to be tiled with identical copies of unit-triangles, such that their corners coincide as springs, sinks and free corners, respectively (Fig. 1).

In addition, we assume blood flow to be identical in all unit-triangles leading to a flow pattern that is repetitive in the section plane like the triangular tiling pattern. Thus computation of blood flow potential can be limited to a single unit-triangle.

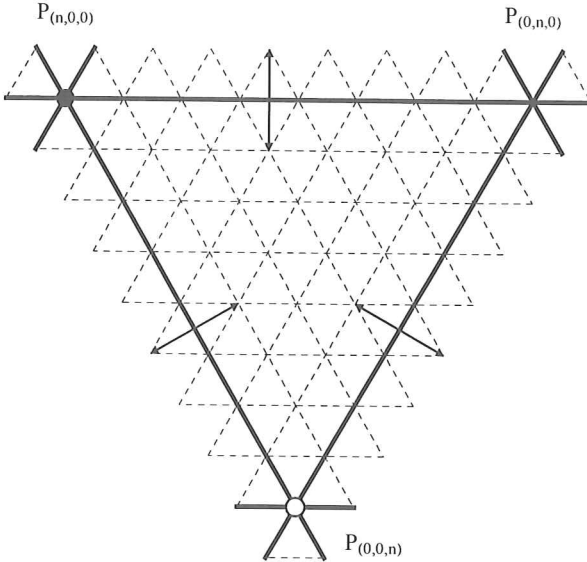


*Fig. 2. Unit-triangle with superimposed triangular grid. Bold lines: Edges of the unit-triangle. Blood flow is assumed to take place exclusively along the edges of the triangular grid (dashed lines), starting at the spring (dark spot, labeled  $P_{n,0,0}$ ) and ending at the sink (white spot,  $P_{0,0,n}$ ). Free corner labeled  $P_{0,n,0}$ . At the unit-triangle border, neighboring grid knots are identified with interior knots to establish symmetric continuation (arrows). For computation, all grid knots are labeled in barycentric coordinates as some  $P_{i,j,k}$  ( $i, j, k \in \{0, \dots, n\}$ ;  $i + j + k = n$ ). Labels of spring, sink, and free corner explicitly given as examples.*

To simplify calculation, we subdivide the unit-triangle by a triangular grid of fixed mesh size ( $n=8$  in this paper) and assume that blood flow takes place exclusively along the edges of the grid (Fig. 2). A conductivity index is attributed to each grid edge giving a (discrete) conductivity distribution inside the unit-triangle. Together with explicitly given spring and sink pressures, blood flow potential on the grid is then completely determined. To compute the flow potential at each grid knot, the solution of a linear equation system is required, as explained in the appendix. As an approximation of the real and continuous flow potential, our discrete model allows to relate intralobular blood flow with the distribution of metabolic activity inside a liver section.

## RESULTS

A physiological model (Fig. 3) was calculated with a portal pressure of 8.9 mmHg (1 mmHg = 133 Pa = 1.36 cm H<sub>2</sub>O) and a venous pressure of 8.7 mmHg following Lauth *et al.* (1986). Initially, an indexed flow conductivity was set at all grid edges to the same value '1'. For taking presinusoidal vessels into account, we changed indices at the triangle border between spring and free corner to a value of '10' (Fig. 3a). Further, width and straightness of the sinusoids increasing from lobular periphery to the center were modeled by a linear increase of indices from '1' to '2' towards the sink. This increase was based on measurements of sinusoid diameter enlargement from lobular periphery to the center of about 20% (Wisse *et al.*, 1985) and the assumption of a diameter-conductivity-relationship as in Hagen and Poiseuille's law (conductivity proportional to diameter in the power of 4).

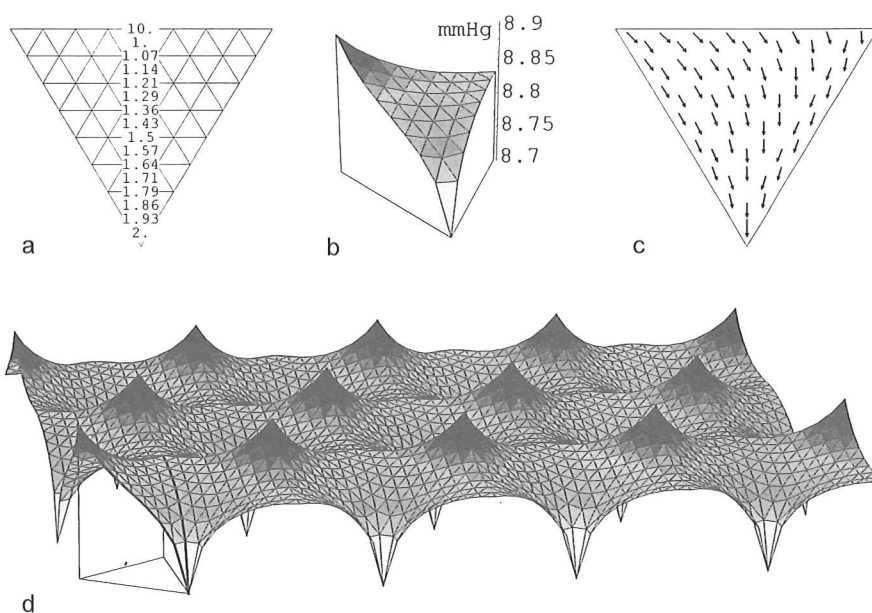


**Fig. 3.** Physiological model. Spring pressure 8.9 mmHg, sink pressure 8.7 mmHg. (a) Conductivity index distribution of the unit-triangle. Each number labels the conductivity index for all edges of the grid with the same vertical position: Index '10' for edges connecting spring and free corner, other indices increase linearly from '1' to '2' from periphery towards the sink. (b) Flow potential surface of unit-triangle (linear interpolation of computed potentials at the grid knots). Shading and surface height both represent local blood flow potential. (c) Gradient field. Arrows indicating direction of local blood flow. (d) Potential surface of the section plane. Unit-triangles positioned as in Fig. 1 (most left and anterior unit outlined), surface height coded as in (b). Springs appear as peaks, sinks as troughs. Free corners are saddle points of the surface. Areas of similar potentials appear in similar shading.

Computation then shows springs and sinks as peaks and troughs in a potential surface (Fig. 3b). Pressure falls with distance from the spring, but the decrease is small in the direction to the free corner as a result of the elevated flow conductivity along that triangle side. In the corresponding gradient field (Fig. 3c), each vector indicates size and direction of the local pressure change and therefore gives the direction of local blood flow. The potential surface of the section plane (Fig. 3d) shows free corners of the unit-triangles as saddle points in the surface. Their potential is considerably closer to the spring than to the sink. The surface can be partitioned in two regions. A continuous region of high potential connects springs and saddle points and forms rings around sinks (darker shading). Here blood is distributed to the lobular periphery. The remaining isolated regions with lower potential (lighter shading), in contrast, show almost concentric blood flow towards the sinks.

In liver congestion hepatic venous pressure and portal pressure are increased. We simulated this condition with a spring pressure of 10 mmHg and a sink pressure of 9.5 mmHg, cf. Lauth et al. (1986). Enlargement of pericentral sinusoids under chronically elevated venous pressure was modeled by linearly increasing (from '1' to '5') the conductivity indices from periphery to the lobular center (Fig. 4a).

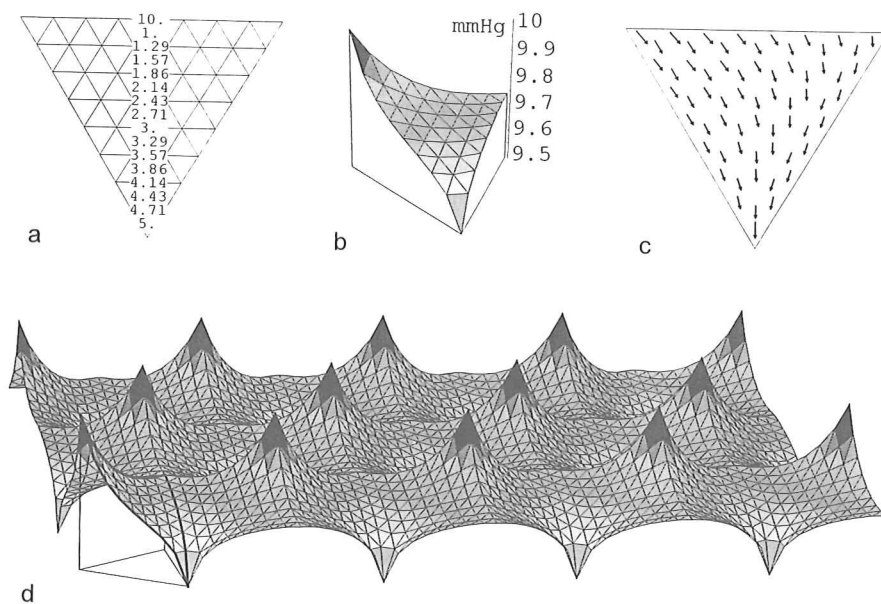


Fig. 4. Liver congestion model. Spring pressure 10 mmHg, sink pressure 9.5 mmHg. (a) Conductivity index distribution in the unit-triangle: Index '10' for edges connecting spring and free corner; linearly increasing indices from '1' to '5' from periphery to the sink. (b) Flow potential surface of one unit-triangle. Shading represents surface height. (c) Gradient field. Arrows indicating direction of local blood flow. (d) Potential surface of the section plane. Unit-triangles (most left and anterior outlined) positioned like in Fig. 1. Please notice the height of the saddle points (in relation to springs and sinks) considerably lower for liver congestion than for the physiological condition (Fig. 3d).

Changes in (explicitly given) spring and sink pressures only shift and scale the potential field. In contrast, modification of flow conductivity leads to a nonlinear reshaping of the potential surface (Fig. 4b). Unlike the physiological condition with a high-level plateau and funnel-like regions near the sinks (Fig. 3d), the model of liver congestion shows a potential surface with sharper peaks at the springs and with saddle points located almost in the middle between spring and sink potentials (Fig 4d). Therefore the regions of homogeneous and concentric blood flow around the sinks are substantially reduced, as compared to the physiological condition.

## DISCUSSION

The presented potential model is based on an equilateral triangle and assumes regular shaped lobules, which are neither realized in pigs nor humans (Leder et al., 1991; Scherberger and Leder, 1997). The model can be interpreted in the sense of the well-established planar central vein lobule, the (complementary) peribiliary lobule, and of Rappaport's (1954) acinus (Fig.1). However, with some perturbations, it could be imagined that unit-triangles can fill a section plane also in more irregular patterns.

Literature reports portal pressures in a range from 4.4 to 9 mmHg, and hepatic venous pressures from 1.1 to 8.7 mmHg (Ayuse et al., 1994; Greenway and Lauth, 1989; Laine et al., 1979; Lauth et al., 1986; McCuskey and Reilly, 1993; Mitzner, 1974; Nakata et al., 1960). Our simulation mainly follows Lauth et al. (1986). However, only the conductivity distribution and the difference between spring and sink pressure determine the shape of the potential surface. Alternative computation (not shown; portal pressure: 7 mmHg, venous pressure: 6 mmHg) as suggested by Laine et al. (1979) resulted in a similar potential surface just shifted and scaled in the vertical (pressure) direction.

For the simulation of liver microcirculation, our model takes into account a two-dimensional morphological heterogeneity. Modification of conductivity at grid edges allows the modeling of the more isotropic sinusoidal network in the periphery and the more concentric directions of such vessels around the lobule center.

In humans, terminal hepatic arteries exclusively terminate in peripheral sinusoids, i.e. in the high area of our potential surface (Yamamoto et al., 1985). In these terminal arteries, the current functional concept assumes a pressure reduction to the pressure level of the terminal portal veins by means of a myogenic autoregulation (Lauth and Greenway, 1987). Accordingly, the inflow pressure of the terminal hepatic arteries into the sinusoids equals the terminal portal pressure. We therefore find it reasonable for our model not to treat arterial and portal inflow separately (i.e. as two sources of blood inflow and with two different pressure levels), but to assume one common source of hepatic blood inflow instead.

Comparisons of our model with oxygen pressure gradients seem to support Rappaport's et al. (1954) concept of the liver acinus. Biochemical studies often refer to this acinar concept of three zones, though in many cases only peripheral and perivenous zones are distinguished (Evans et al., 1990; Gascon-Barré et al., 1992; Häussinger, 1983; Morimoto et al., 1993). The two-dimensional metabolic model of Lamers et al. (1989), however, consists of three zones arranged in a hexagonal grid. It fits our simulations, if their outer, middle, and inner zones are identified with regions of high, intermediate, and low potential.

Teutsch (1988) describes hepatic glucose-6-phosphatase distributions with an activity gradient along the lobular edge besides a stronger fall to the lobular center. His two-dimensional activity diagrams show saddle points alternating with portal tracts at the lobular periphery. They correspond to saddle points in our potential surface model. This coherence

strongly emphasizes a close relationship between microvascular blood flow and metabolic heterogeneity.

For simulation of liver congestion, we assumed a pressure of 8 mmHg in the systemic venous circulation (V. cava inf.). Following Lauth et al. (1986), this leads in the cat to a portal vein pressure of 10 mmHg and a hepatic vein pressure of 9.5 mmHg. In contrast, Laine et al. (1979) reported in dogs for the same systemic pressure condition a portal pressure of 12 mmHg and estimated lobar hepatic vein pressures to about 10 mmHg. Simulations with these alternative pressures (but identical conductivity distribution) resulted in a potential surface just shifted and scaled (not shown).

How much sinusoids enlarge under liver congestion is hardly known. Clearly, sinusoids close to the central vein are more enlarged than periportal sinusoids, but quantitative data were not present. For a first, rather qualitative approach, we increased the indexed conductivity in our model somewhat arbitrarily by a factor of 5 from periphery to center.

The observed changes in liver histology reflect the alterations of the simulated flow potential. Regions of dilated sinusoids, also known under the old German pathological term "Stauungsstrassen" ['congestion streets'], extend from one pericentral area to its neighbors. They correspond to regions of low potential connecting neighboring sinks via saddle points in the potential surface. The increased pericentral conductivity leads to a decreased pressure gradient from the sink to the saddle point and could explain why in pathological studies blood congestion is found particularly in these regions.

Our two-dimensional model of hepatic blood flow potential complies with up-to-now exclusively two-dimensional descriptions of liver microcirculation and metabolism. Considering the multiple cross-connections in the sinusoidal network, flow conditions are highly correlated between adjacent section planes. Our two-dimensional results might therefore still be valid in a three-dimensional model extension. Such an extension, however, should incorporate a three-dimensional model of lobular architecture as an essential part.

## REFERENCES

- Ayuse T, Brienza N, O'Donnell CP, Robotham JL. Pressure-flow analysis of portal vein and hepatic artery interactions in porcine liver. *Am. J. Physiol* 1994; 267: H1233-H1242.
- Eisenberg J. Physiologie der Leber. In *Physiologie des Menschen.*, vol. 8 (ed. K. Gauer, Jung), pp. 219-244. München: Urban & Schwarzenberg, 1972.
- Evans JL, Quistorff B, Witters LA. Hepatic zonation of acetyl-CoA carboxylase activity. *Biochem J* 1990; 270.
- Gascon-Barré M, Vallières S, Benbrahim N, Huet PM. C-25 hydroxylation of vitamin D3 in periportal and perivenous region of hepatic acinus. *Am J Physiol* 1992; 262: 810-817.
- Greenway CV, Lauth WW. Hepatic circulation. In *Handbook of Physiology. Section 6: The Gastrointestinal System* (ed. J. D. Wood), pp. 1519-1564. Bethesda, Maryland: American Physiological Society.
- Häussinger D. Hepatocyte heterogeneity in glutamine and ammonia metabolism and the role of an intercellular glutamine cycle during urogenesis in perfused rat liver. *Euro J Biochem* 1983; 133: 269-275.
- Laine G, Hall JT, Laine SH, Granger, HJ. Transsinusoidal fluid dynamics in canine liver during venous hypertension. *Circ.Res.* 1979; 45: 317-323.
- Lamers WH, Hilberts A, Furt E, Smith J, Jonges GN, van Noorden JF, Gaasbeek Janzen JW, Charles R, Mooreman AF. Hepatic enzymatic zonation: A re-evaluation of the concept of the liver acinus. *Hepatology* 1989; 10: 72-76.

- Lautt WW, Greenway CV. Conceptual review of the hepatic vascular bed. *Hepatology* 1987; 7: 952-963.
- Lautt WW, Greenway CV, Legare DJ, Weisman H. Localization of intrahepatic portal vascular resistance. *Am. J. Physiol.* 1986; 251 G: 375-381.
- Leder O, Scherberger H, Kurz H, Müller H. Modelling of the liver. In *MIE'91 Satellite Conference on Computer Modelling and National Meeting on Biomedical Informatics.*, pp. 13-21. Budapest: Hungary, 1991 (ISBN 9638431733).
- McCuskey RS, Reilly FD. Hepatic microvasculature: dynamic structure and its regulation. [Review]. *Seminars in Liver Disease* 1993; 13: 1-12.
- Mitzner W. Hepatic outflow resistance, sinusoid pressure, and vascular waterfall. *Am. J. Physiol.* 1974; 227: 513-519.
- Morimoto Y, Wettstein M, Häussinger D. Hepatocyte heterogeneity in response to extracellular adenosine. *Biochem J* 1993; 293: 573-581.
- Nakata K, Leong GF, Brauer RW. Direct measurement of blood pressures in minute vessels of the liver. *Am. J. Physiol.* 1960; 199: 1181-1188.
- Prandtl L. *Strömungslehre*. Braunschweig: Vieweg & Sohn, 1956.
- Rappaport AM, Borowy ZJ, Loughheed WM, Lotto WN. Subdivision of hexagonal liver lobules into a structural and functional unit. *Anat. Rec.* 1954; 119: 11-33.
- Scherberger H. Das Leberläppchen des Schweines: Quantitative Analyse von Schnittbildern und räumlichen Rekonstruktionen. 2D-Modellierung der Blutströmung. Freiburg: Albert-Ludwigs-Universität, 1996.
- Scherberger H, Leder O. Section topology and 3d-visualization of pig liver lobules. *Acta Stereologica* 1997; 16: 111-118.
- Teutsch HF. Regionality of glucose-6-phosphate hydrolysis in the liver lobule of the rat: Metabolic heterogeneity of portal and septal sinusoids. *Hepatology* 1988; 8: 311-317.
- Wisse E, De Zanger RB, Charles K, Van der Smissen P, McCuskey RS. Presinusoidal and proximal intrasinusoidal confluence of hepatic artery and portal vein in rat liver: Functional evidence by orthograde and retrograde bivascular perfusion. *Hepatology* 1985; 5: 683-692.
- Wolfram S. *Mathematica*. Reading, Mass.: Addison-Wesley, 1991.
- Yamamoto K, Sherman I, Phillips MJ, Fisher MM. Three-dimensional observations of the hepatic arterial termination in rat, hamster and human liver by scanning electron microscopy of microvascular casts. *Hepatology* 1985; 5: 452-456.

**APPENDIX: COMPUTATIONAL METHODS**

For a given unit-triangle a triangle grid oriented to the triangle sides is superimposed, such that the grid subdivides each edge in  $n$  ( $n = 8$  in this paper) equally spaced intervals (Fig. 2). Using a barycentric coordinate system, the knots of the grid can be written as  $P_{(i,j,k)}$  with  $i, j, k \in \{0, \dots, n\}$  and  $i + j + k = n$ . For example,  $P_{(n,0,0)}$  may denote the spring location, while  $P_{(0,n,0)}$  and  $P_{(0,0,n)}$  label the free corner and the sink of the unit-triangle, respectively.  $U_{(i,j,k)}$  may give the flow potential in  $P_{(i,j,k)}$ .

Neighbors of a knot  $P_{(i,j,k)}$  can be written as  $P_{(i,j,k)+\nu}$ , if  $\nu \in \Pi$  and  $\Pi$  is the set of permutations of the triple  $(1, -1, 0)$ . Further, the conductivity index of a grid edge connecting two knots  $P_{(i,j,k)}$  and  $P_{(i,j,k)+\nu}$  may be symbolized as  $L_{(i,j,k)+\frac{1}{2}\nu}$  (index chosen as barycentric coordinates referring to the center of the grid edge).

To describe symmetric continuation at the sides of the unit-triangle, the grid and the barycentric coordinate system is slightly extended to neighboring unit-triangles and the following knots identified (Fig. 2):

$$P_{(-1,j,k)} = P_{(1,j-1,k-1)} \tag{1}$$

$$P_{(i,j,-1)} = P_{(i-1,j-1,1)} \tag{2}$$

$$P_{(i,-1,k)} = P_{(i-1,1,k-1)} \tag{3}$$

These equations are valid for all indices such that  $i, j, k \in \{0, \dots, n\}$  and the sum of each index triple is  $n$ . Similar equations are assumed for flow potentials  $U_{(i,j,k)}$  and conductivities  $L_{(i,r,t)}$ . To discretize the problem, we assumed blood flow taking place only on the grid. Then computation of the flow potential means the calculation of all  $U_{(i,j,k)}$ , given the conductivity indices  $L_{(i,r,t)}$  and the explicit spring and sink potentials  $U_{(n,0,0)}, U_{(0,0,n)}$ .

Potential theory states that at each knot being not a spring or a sink, the sum of all (signed) flows is zero. In our notation:

$$\sum_{\nu \in \Pi} I_{\nu} = 0 \tag{4}$$

for a knot  $P_{(i,j,k)}$  and flows  $I_{\nu}$  going to the neighboring knots  $P_{(i,j,k)+\nu}$ .

Using  $p = (i, j, k)$  and the flow equation  $I = \Delta U \cdot L$  ( $I$  flow,  $\Delta U$  potential difference and  $L$  conductivity), a flow  $I_{\nu}$  from a knot  $P_p = P_{(i,j,k)}$  to a knot  $P_{p+\nu}$  can be expressed as

$$I_{\nu} = (U_p - U_{p+\nu}) L_{p+\frac{1}{2}\nu} \tag{5}$$

Using (4), summation over all  $I_{\nu}$  at  $P_p$  results in

$$0 = \sum_{\nu \in \Pi} I_{\nu} = \sum_{\nu \in \Pi} (U_p - U_{p+\nu}) L_{p+\frac{1}{2}\nu} \tag{6}$$

Rearrangement of this equation and constraint considerations at spring and sink locations then lead to the following linear equation system:

$$U_{(n,0,0)} = \text{portal pressure} \tag{7}$$

$$U_{(0,0,n)} = \text{venous pressure} \tag{8}$$

$$U_p \sum_{\nu \in \Pi} L_{p+\frac{1}{2}\nu} = \sum_{\nu \in \Pi} U_{p+\nu} L_{p+\frac{1}{2}\nu} \tag{9}$$

Equation (9) is valid for all  $p = (i, j, k)$  with  $i, j, k \in \{0, \dots, n\}$ ,  $i + j + k = n$ ,  $p \neq (n, 0, 0)$ ,  $p \neq (0, 0, n)$ , and equations (1-3) expressing symmetrical continuation applied to all variables  $U_{p+v}$  and  $L_{\frac{p+v}{2}}$  outside the unit-triangle.

Under these constraints, equation system (7-9) consists of  $(n+1)(n+2)/2$  equations and an equal number of unknowns  $U_{(i,j,k)}$ . As conductivity indices are strictly positive, a unique solution exists and can be obtained by using standard procedures for the solution of linear equation systems, like given in Wolfram (1991).

Implementation was done in Mathematica 2.0 for the Macintosh.

*Accepted: 18 October 1998*